arXiv:1509.08412v2 [cond-mat.mtrl-sci] 20 Nov 2015

# How the aggregation of oxygen vacancies in rutile based $TiO_{2-\delta}$ phases causes memristive behavior.

Wolfgang Heckel,[1,*] Michael Wehlau,[2] Sascha B. Maisel,[1]
Thomas Frauenheim,[2] Jan M. Knaup,[2,†] and Stefan Müller[1]

[1] *Institute of Advanced Ceramics, Hamburg University of Technology, D-21073 Hamburg, Germany*

[2] *Bremen Center for Computational Materials Science, University of Bremen, D-28359 Bremen, Germany*

(Dated: November 23, 2015)

## Abstract

The results of a comprehensive and systematic ab-initio based ground-state search for the structural arrangement of oxygen vacancies in rutile phase $TiO_2$ provide new insights into their memristive properties. We find that O vacancies tend to form planar arrangements which relax into structures exhibiting metallic behavior. These meta-stable arrangements are structurally akin to, yet distinguishable from the Magnéli phase. They exhibit a more pronounced metallic nature, but are energetically less favorable. Our results confirm a clear structure-property relationship between segregated oxygen vacancy arrangement and metallic behavior in reduced oxides.

## I. INTRODUCTION

Understanding the behavior of O vacancy defects ($V_O$) in reducible metal oxides is of paramount importance to understanding a wide range of highly interesting physical and chemical effects. These include oxide catalysis for sustainable $CO_2$ conversion into chemical fuels, highly efficient batteries for sustainable energy storage and electromobility, and innovative electronic devices with the potential to fundamentally transform information technology. The latter is expected to be enabled by the memristor, a fascinating new electronic device that complements the widely known passive two-terminal devices of resistor, capacitor and inductance[1,2]. It acts as an ohmic resistance depending on the history of the current which has flown through it in the past—hence the name which is a contraction of memory and resistor. Already proposed in the 1970s by Chua[1], the purposeful implementation of memristors could only be achieved in 2008[3]. Memristors are being considered for two main applications: First, resistive switching memory will to scale far beyond current FLASH memory technology[4,5], which relies on tunneling electrons to and from floating gates in CMOS transistors. From this arises the possibility to shift computing paradigms away from the current compute centric Von Neumann architecture towards storage centric concepts[6] which avoid data transfer bottlenecks in the former. Second, the memristor forms an indispensable building block of electronic analogues to nerve cells for neuromorphic computing[7,8]. Without it, modeling synaptic behavior requires extremely complex active electronics. This complexity severely limited the possible number of interlinks between artificial neurons, rendering the construction of powerful neuromorphic devices infeasible. Recently, an artificial neuronal network was implemented in hardware, interlinking 576 artificial neurons in Si based CMOS by a matrix of 73728 artificial synapses realized by WO memristors on the same chip[9]. The device exhibits considerable learning ability and constitutes a significant advance in neuromorphic computing. At the same time, enormous effort is exerted in the development of resistive switching memory based on transition metal oxide memristors. Laboratory devices already surpass speed and durability of FLASH memory cells[5].

The first material in which memristors were implemented was $TiO_{2-\delta}$ and it is still an enormously useful and interesting model system[3]. It is understood that the resistance modulation is based on the migration of oxygen vacancy defects and the formation and dissolution of conductive[10] Magnéli phases[11,12] which are based on planar arrangements of

oxygen vacancies ($V_O$) in the rutile structure and have $Ti_nO_{2n-1}$ stoichiometry[13,14]. High precision theoretical calculations[15] have shown that electrical conductivity can be induced in rutile by different kinds of vacancy arrangements, bearing only marginal resemblance to Magnéli phases. However, this earlier study was limited to a small number of examined vacancy arrangements by the prohibitive computational cost of ab-initio methods that can describe the electronic structure of $V_O$ in $TiO_2$[16]. Still, combined with the finding that rutile is severely destabilized by oxygen deficiency, as evidenced by a pronounced reduction in melting temperature[17], these results lead to an important question for the understanding of the memristive effect in transition metal oxides in general: Is the observed formation of Magnéli phases prerequisite for the effect or is the resistance change caused by a larger class of structural features, with the Magnéli phase being the thermodynamically most favorable structure exhibiting these features?

With an exhaustive ground-state search, attained by a density functional theory (DFT) based cluster expansion (CE) approach, we shed light on that question. In this letter, we present the first systematic investigation of the full configuration space for $V_O$ in $TiO_2$ rutile. We identified planar $V_O$ arrangements to be energetically relevant and responsible for the metallic behavior in reduced oxides.

## II. METHODS

In order to explore the full configuration space of $V_O$ ordering in reduced $TiO_2$ rutile, we initiated a cluster expansion (CE)[18] using the UNCLE code[19] in the $V_O$ concentration range of $0 \ldots 16.7\,\%$. The total energies of the CE input structures were determined by DFT calculations employing VASP[20,21]. We have applied the PAW-GGA[22,23] functional PBEsol[24] with a conjugate gradient algorithm to relax the structures with respect to cell volume, cell shape and atomic positions until the forces on each atom were smaller than $5\,\mathrm{meV/Å}$. The energy cutoff of the plane-wave basis was set to $520\,\mathrm{eV}$. To keep the computational effort within tractable limits, the considered cells were restrained to every possible unit cell of O defective rutile containing 10 or less Ti atoms.[25] Every such cell predicted to be energetically favorable by the CE was calculated by DFT (cf. Fig. 1).

For the examination of the density of states, additionally, the geometries of selected structures were relaxed by applying the polaron correction developed by Lany and Zunger[26–28]

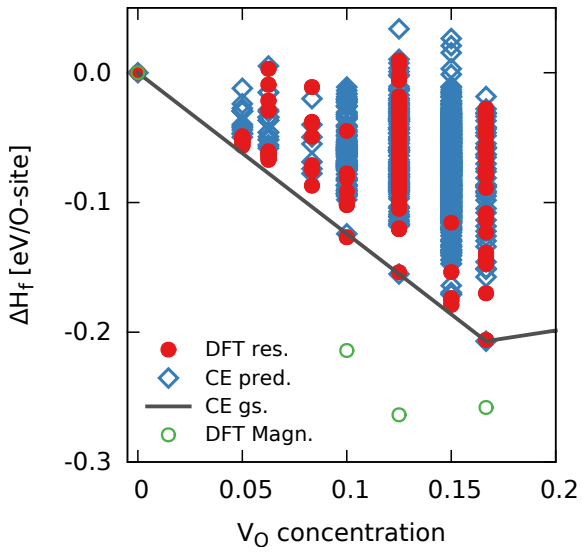


FIG. 1: (color online) Formation enthalpies $\Delta H_\mathrm{f}$ (see Eq. 4) of vacancy orderings in the rutile crystal structure resulting from a DFT based (filled red circles) CE fit (open blue squares). The black solid line marks the CE ground states. For comparison, the DFT formation enthalpies of the Magnéli phase are also displayed (open green circles).

and, subsequently, a static HSE06[29,30] calculation approximates the electronic ground state. In their polaron correction, Lany and Zunger introduce the additional potentials

$$V_\mathrm{hs} = \lambda_\mathrm{hs}\,(1 - n_{m,s}/n_\mathrm{O,rutile}) \tag{1}$$

for hole states and

$$V_\mathrm{es} = \lambda_\mathrm{es}\,(1 - p_{m,s}/p_\mathrm{Ti,rutile}) \tag{2}$$

for electron states to satisfy Koopmans theorem. $n_{m,s}$ and $p_{m,s}$ are fractional occupancies of state $m$ with spin $s$, $n_\mathrm{O,rutile}$ and $p_\mathrm{Ti,rutile}$ denote the occupancies in undisturbed, defect-free $TiO_2$ rutile, and $\lambda$ defines the coupling. We set these potentials for O 2p hole states to $\lambda_\mathrm{hs} = 4.81\,\mathrm{eV}$ and Ti 3d electron states to $\lambda_\mathrm{es} = 4.18\,\mathrm{eV}$.[31] Applying the polaron correction, only subtle differences in defect geometries occur, which however might have a strong impact on hybrid exchange band structures.

The Brillouin zone sampling of all structures, independent of cell shape or size, was performed using a $7 \times 7 \times 7$ MonkhorstPack[32] mesh for PBEsol and Lany-Zunger corrected calculations, and a $3 \times 3 \times 3$ mesh for HSE06 calculations.

The CE Hamiltonian

$$E(\sigma) = \sum_{C \in \mathbf{C}} J_C \Pi_C(\sigma) \tag{3}$$

expands the energy of a given structure $\sigma$ into a sum over $n$-body correlation functions $\Pi_C(\sigma)$ times expansion coefficients $J_C$. A genetic algorithm elaborated in Refs. 33 and 34 is used to truncate the sum of Eq. 3 and reduce it to the most relevant $n$-body interactions. Then, the expansion coefficients $J_C$ of this optimized set $\mathbf{C}$ are extracted by fitting them to a first-principles data base. A cross-validation scheme[35] is used to control the error of the fits.

The CE Hamiltonian can then be used to evaluate the energetics of more than 300 000 structures quickly and efficiently. Whenever the CE Hamiltonian predicts a structure to be energetically more favourable than the DFT input structures, it is relaxed with DFT and added to the input set for the next iteration of the CE. This procedure is reiterated until the CE is self-consistent. The quality of the fits is observed to vary smoothly with the number of input structures and the number of non-zero $n$-body interactions.

The final CE yielding the results shown in this paper uses a grand-total of 143 input structures, including the pure elements. The fit incorporates 35 interactions as determined by the genetic algorithm, which can be found in the supplement. The Hamiltonian yields a cross-validation score of 8.9 meV/O-site. This ensures a sufficient accuracy for the CE energy predictions.

Formation enthalpies in Figure 1 are calculated according to

$$\Delta H_\mathrm{f} = E(\sigma) - x \cdot E(100\,\%\ \mathrm{V_O}) - (1-x) \cdot E(\mathrm{TiO_2\ rutile}), \tag{4}$$

where $E(\sigma)$ denotes the total energy of structure $\sigma$ and $x$ the $\mathrm{V_O}$ concentration of that structure. $E(\mathrm{TiO_2}$ rutile) and $E(100\,\%\ \mathrm{V_O})$ correspond to the perfect stoichiometric $\mathrm{TiO_2}$ rutile ($0\,\%\ \mathrm{V_O}$) and the 100 % vacancy pseudo-element concentration energy, respectively. To identify energetically favorable $\mathrm{V_O}$ orderings, we assign the total energy of a $\mathrm{TiO_2}$ rutile structure without any oxygen atoms to $E(100\,\%\ \mathrm{V_O})$. This leads to apparent ground states at intermediate vacancy concentrations, as displayed in Fig. 1. As one expects, no ground state between perfect $\mathrm{TiO_2}$ rutile ($0\,\%\ \mathrm{V_O}$) and pure Ti ($100\,\%\ \mathrm{V_O}$) would appear if the total energy of hcp-Ti were assigned to the $100\,\%\ \mathrm{V_O}$ structure.

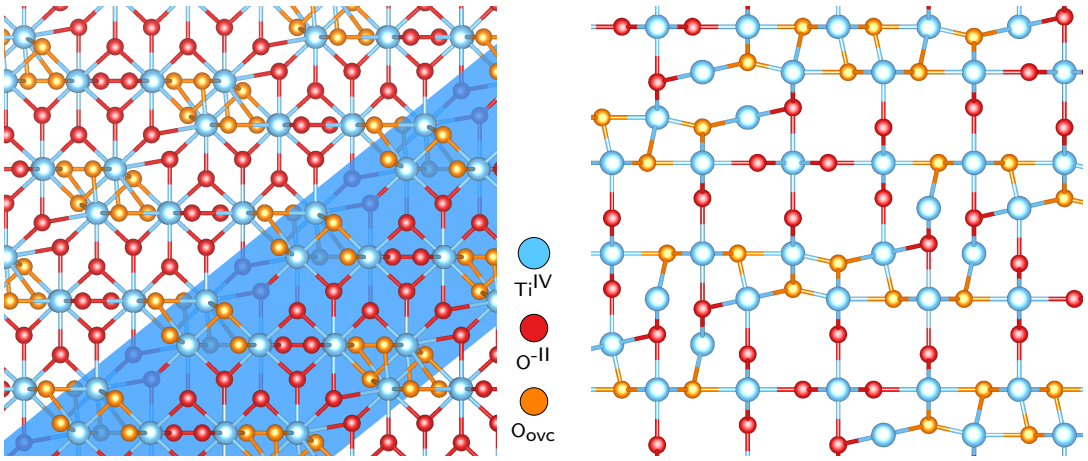


(a) view in [111]

(b) (001) view, for clarity one layer only

FIG. 2: (color online) Relaxed $Ti_4O_7$ Magnéli structure. Overcoordinated $O_{ovc}$ atoms (orange) form quasi-one-dimensional channels in [111]. All Ti atoms (blue) retain 6-fold coordination. Fully coordinated oxygen atoms appear in red. The crystallographic (121) shear plane (see text for affinity to rutile) is marked blue.

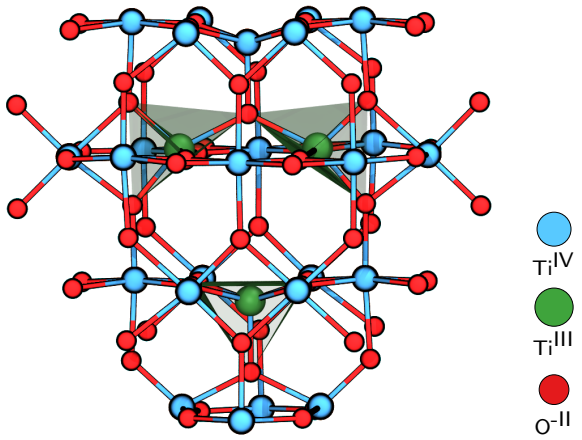


FIG. 3: (color online) Relaxed structure of the isolated $V_O$ arrangement predicted for 5 % $V_O$ concentration. The missing oxygen atom induces three undercoordinated $Ti^{III}$ ions, marked in green.

## III. RESULTS

### A. Structural Features and Thermodynamic Stability

Among all structures considered in this study, three classes attract particular attention due to their energetic appearance in the ground-state diagram (Fig. 1):

1. The Magnéli structures $Ti_5O_9$, $Ti_4O_7$, $Ti_3O_5$, into which none of the structures considered in the CE study can relax directly. Having calculated their fully relaxed DFT energy separately, they appear to be energetically most favorable.

2. Meta-stable arrangements, having evenly distributed vacant O sites separated by at least one occupied site in every direction. These structures consistently exhibit formation enthalpies notably above the CE ground-state line.

3. Structures with a certain low-dimensional $V_O$ ordering (see below for a detailed description), energetically outmatching all other $V_O$ arrangements covered by the CE study. They are detected at 10 %, 12.5 %, and 16.7 % $V_O$ and form the energetic ground-state line (apart from the Magnéli structures mentioned above) exhibiting a considerable energy gap with regard to all other structures.

$Ti_nO_{2n-1}$ Magnéli structures are made up of $TiO_2$ rutile blocks, which are periodically interrupted at (121) shear planes[36,37]. The crystallographic operation to move a rutile block from its perfect rutile position to its Magnéli phase position is $(121)_{\text{rutile}}\frac{1}{2}[0\bar{1}1]_{\text{rutile}}$ relative to its neighboring rutile block. By deleting overlapping oxygen atoms one obtains the $Ti_nO_{2n-1}$ stoichiometry. The higher the $n$, the larger is the block of perfect rutile between two shear planes.

Fig. 2 shows the relaxed $Ti_4O_7$ Magnéli structure, which appears energetically most favorable. As in rutile, all Ti atoms retain 6-fold coordination. Slightly expanded quasi-one-dimensional channels of overcoordinated O atoms arrange in [111] direction, separated from each other in $[0\bar{1}1]$ direction just by two regularly coordinated O atoms. These approximatively planar arrangements alternate with narrow undisturbed rutile blocks. While in rutile the Ti octahedra only share edges and vertices, in the characteristic shear planes of the Magnéli phases they share facets.

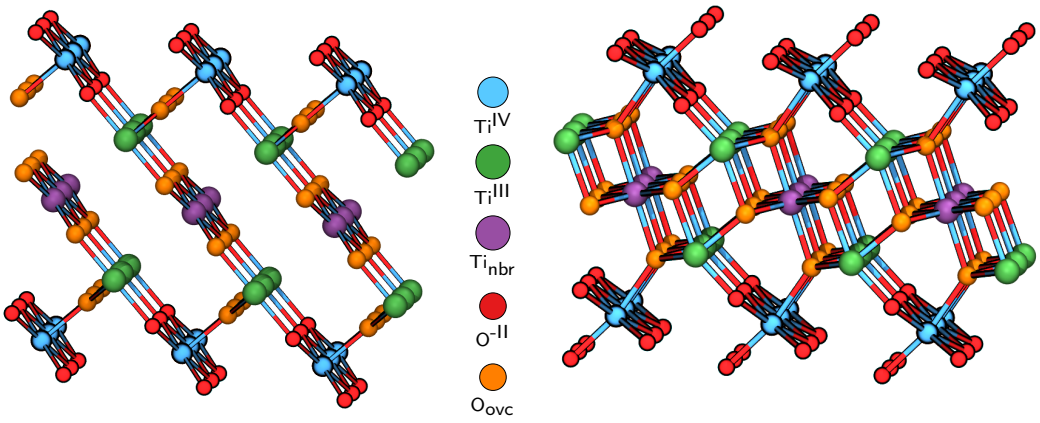


(a) $V_O$ arrangement on rutile lattice prior to relaxation

(b) relaxed structure

FIG. 4: (color online) Planes of $V_O$ relax into $Ti^{III}$ linked by overcoordinated $O_{ovc}$ atoms. For more details and the denotation, see text.

Due to the substantial restructuring from rutile to a Magnéli phase, as described above, extensive energy barriers are expected to hinder transformation into the energetically favorable state. None of the $V_O$ defect structures considered in this CE study can relax into it.

Since the cells that are tractable by DFT in large numbers are limited in size, at low $V_O$ concentration the large portions of undisturbed rutile between separating the $V_O$ agglomerates cannot be modeled. Under these circumstances, the vacant O sites are evenly distributed and separated by at least one occupied site in every direction. In this meta-stable arrangement, the vacancy retains its well known structure surrounded by three truncated TiO octahedra, where the Ti ions are regarded as being in the $Ti^{III}$ oxidation state. Exemplarily, Figure 3 shows the relaxed geometry of the lowest energy structure at 5 % $V_O$ concentration.

For the same reason, higher order Magnéli phases, constructed of $V_O$ layers separated by thick layers of undisturbed rutile, are extremely challenging for computational modeling. Still, from empirical experience, they are expected to be energetically favorable.

At higher vacancy concentrations, we find ordering of vacancies in direct neighborhood on a wide variety, arranged along lines or within slip planes. The prototype of the energetically

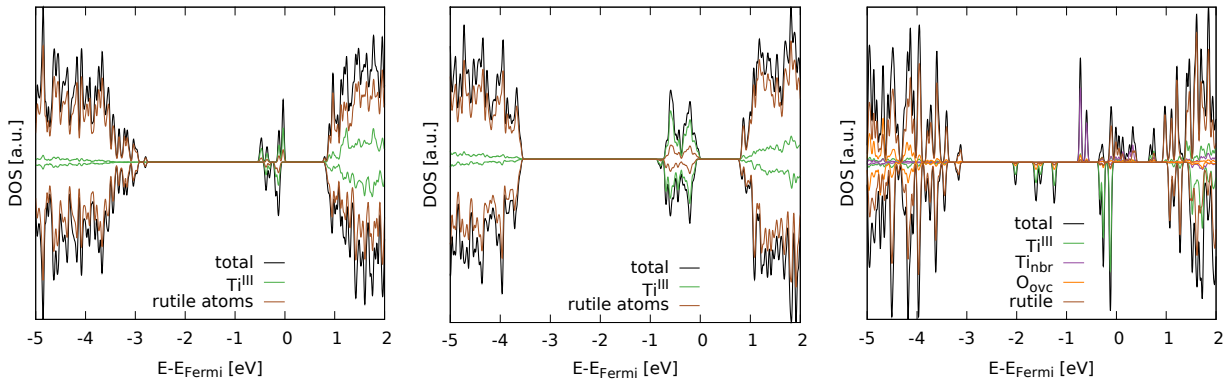


(a) 5 % $V_O$ isolated (b) $Ti_4O_7$ Magnéli phase (c) 16.5 % $V_O$ planar

FIG. 5: (color online) Spin polarized densities of states of isolated $V_O$ (cf. Fig. 3), the Magnéli phase $Ti_4O_7$, and the prototypical planar $V_O$ arrangements found for 16.7% $V_O$ concentration (cf. Fig. 4).

favorable defect structure is a $V_O$ planar arrangement (see Figure 4), detected at 10 %, 12.5 %, and 16.7 % $V_O$. Prior to relaxation, this structure is characterized by two features (Fig. 4a): a (100) $V_O$ double plane, (i.e. $V_O$ double rows in [010] and [001] direction,) formed by missing apex oxygen atoms formerly belonging to one Ti octahedron, and an odd number of undisturbed Ti octahedra in (100) direction. This structure relaxes into the geometry shown in Figure 4b. It is characterized by a layer of five-fold coordinated $Ti^{III}$ ions, linked by overcoordinated $O_{ovc}$ ions.[38] The atoms labeled $Ti_{nbr}$ are those missing two direct O neighbors in the prototype structure. As Figure 4b shows, 6-fold coordination is restored for these atoms. The layered arrangement of $Ti^{III}$, $Ti_{nbr}$ and $O_{ovc}$ found in the most favorable structures of our CE separate slightly shifted blocks of perfect rutile from each other. Thus they are very similar to those found in the Magnéli phases[39,40], lacking the strong atomic restructuring during formation compared to Magnéli phases.

### B. Electronic Properties

Analyzing the densities of states (DOS) of the HSE06 electronic structure calculations performed at the relaxed geometries, we find a very clear trend illustrated in Figure 5: For evenly dispersed $V_O$ (see e. g. arrangement in Fig. 3), the electronic structure resembles

that of isolated vacancies (cf. Fig. 5a). For dense $V_O$ planes (see e. g. arrangement in Fig. 4), we note the appearance of a broad, metallic interband close to the rutile conduction band (Fig. 5c). This band provides high conductivity even at low temperatures. Close examination of the projected DOS shows, that the appearance of this metallic interband is caused by an overlap of defect states originating from $Ti^{III}$ in the $V_O$ layer and states originating from nearby $Ti^{IV}$.

In contrast, the low temperature form of the $Ti_4O_7$ Magnéli phase exhibits a fully occupied band within the gap (Fig. 5b). Our results on the Magnéli phase are in very good agreement with previous calculations by Liborio et al.[39] using DFT+U. Furthermore, they match nicely with the DOS of $Ti_2O_3$ determined by Padilha et al.[41] using DFT+U and HSE. Since the latter study contains DOS of higher order Magnéli structures, too, none of them shows a comparable clearly separated, non-magnetized defect band as the one in Figure 5b.

## IV. DISCUSSION

Although our findings confirm the initial results of Magyari-Köpe et al.[15], we interpret our results with a somewhat different focus. The prohibitive cost of sufficiently precise electronic structure calculations severely limited the structural search space of earlier studies and precluded cell shape relaxation. Our approach, while still involving enormous computational effort and being limited to a certain configuration-space size, allows us to compare all structures of this configuration space instead of few handpicked samples. Thus, we are able to directly prove that segregation of $V_O$ in rutile $TiO_{2-\delta}$ into planes is favorable over a uniform distribution.

Even though our present study is static in nature, the very high migration barriers found in bulk rutile[42], combined with the fact that $TiO_{2-\delta}$ films used in existing devices are grown in the amorphous state, suggest that the transition is not *amorphous→rutile→Magnéli*. We rather expect the vacancy agglomeration to occur in a lower density phase, either amorphous or anatase (the latter having been observed in situ[11]). This distinction, however small, may prove technologically very advantageous. It has been shown[4] that for commercially viable application in nonvolatile memory, the reaction rate constants during switching must be several orders of magnitude larger than during storage or reading. The phase transition to a rutile based structure in the low resistance state, which leads to a strong raise in

$V_O$ migration barriers, facilitates achieving this difference. To understand, and possibly engineer, the switching process and storage behavior of memristive devices, it is paramount to first understand the static, highly stable ON and OFF states. Since we find meta-stable structures with a clearer metallic nature than Magnéli phases, promising better conductivity, it may be technologically beneficial to seek the formation of such a non-Magnéli structure.

Our approach to the cluster expansion simulation of $V_O$ defects in $TiO_2$ is not limited to this specific application, but can be generalized to any situation where vacancy or substitutional defects can reside on a distinct sublattice of a compound material.

The results concerning the $V_O$ ordering in $TiO_2$ show a clear tendency for $V_O$ segregation into planes with a very pronounced energy gap with respect to more disperse distributions. These configurations relax into structures where planes of $Ti^{III}$ ions are linked by $O_{ovc}$ ions. Due to technical constraints, such as limited cell sizes to sustain DFT manageability and ionic relaxation algorithms not being able to overcome arising energy barriers, the experimentally found Magnéli defect planes, could not be reproduced in the CE study. Having restored 6-fold coordination at every Ti atom, the Magnéli structures constitute the ground state—also in this study.

Our detailed analysis based on precise electronic structure calculations shows that there is a definite positive correlation between the structural features of planar $Ti^{III}$ and $O_{ovc}$ ions and the formation of a metallic density of states, as shown in Fig. 5. Interestingly, the Magnéli structure does not exhibit a metallic DOS, but rather a characteristic deep band of occupied states. The meta-stable $V_O$ arrangement shown in Figure 4b exhibits a much more pronounced metallic behavior than any Magnéli phase variant examined in our own work as well as earlier DFT+U studies by Liborio et al.[39].

These findings suggest that the Magnéli phase is not necessarily a prerequisite for the high conductive state of a memristor. Due to the relatively high $V_O$ mobility compared to Ti[42], planar $V_O$ aggregation may happen first, already causing distinct conductivity. Subsequently, the actual ground state—the Magnéli phase—may arise by shifting the rutile layers among the $V_O$ planes and finally form the long-lasting low-resistance state.

Further, the results cast some doubt upon the identification of the crystal structure of the conductive filaments in on-state memristor devices as Magnéli phases. The relaxed planar $V_O$ arrangements are structurally very similar to the Magnéli phase. Specifically, both phases exhibit the same arrangement of disturbed planes at the same inter-plane distances.

This makes the distinction between the Magnéli phase and the planar $V_O$ arrangements found in our CE calculations extremely challenging.

## V. CONCLUSION

In summary, we performed a broad and systematic study of the thermodynamics of $V_O$ arrangements in rutile $TiO_2$, combined with highly accurate electronic structure analysis of the most favorable structures. Our results are in accordance with previous experimental reports indicating a preferential $V_O$ segregation into planar arrangements[12], and confirm the earlier hypothesis that these arrangements cause the observed high conductivity[15]. The Magnéli phase does not seem to be a mandatory prerequisite for the low resistive state of memristors. Some contradictions between the calculated electronic structure of the Magnéli phase and observed metallic behavior point to two open fundamental questions: On the theoretical side, precise and detailed band structure calculations of the Magnéli phase are needed, while experimentally it must be endeavored to distinguish between the Magnéli phase and other planar $V_O$ arrangements.


### ACKNOWLEDGMENTS

We gratefully acknowledge financial support from the German Research Foundation (DFG) via SFB 986 "M$^3$", project A4. J.M.K. is grateful for a grant in the "own position" program by the German Research Association (DFG). Atomic structure representations were created using VESTA[43] and VMD[44]. CE was performed using the UNCLE code[45]. The authors thank Dr. Peter Deák for intensive discussion about properties and simulation of $V_O$ defects in $TiO_2$.


---


* wolfgang.heckel@tuhh.de

† now: Atotech Deutschland GmbH, Berlin, Germany



[1] L. O. Chua, IEEE T. Circuits Syst. **18**, 507 (1971).

[2] L. Chua, Appl. Phys. A: Mater. **102**, 765 (2011).

[3] D. B. Strukov, G. S. Snider, D. R. Stewart, and R. S. Williams, Nature **453**, 80 (2008).

[4] R. Waser, R. Dittmann, G. Staikov, and K. Szot, Adv. Mater. **21**, 2632 (2009).

[5] S. Clima, K. Sankaran, Y. Y. Chen, A. Fantini, U. Celano, A. Belmonte, L. Zhang, L. Goux, B. Govoreanu, R. Degraeve, D. J. Wouters, M. Jurczak, W. Vandervorst, S. D. Gendt, and G. Pourtois, Phys. Status Solidi RRL **8**, 501 (2014).

[6] D. B. Strukov, D. R. Stewart, J. Borghetti, X. Li, M. Pickett, G. M. Ribeiro, W. Robinett, G. Snider, J. P. Strachan, W. Wu, Q. Xia, J. J. Yang, and R. S. Williams, in *Circuits and Systems (ISCAS), Proceedings of 2010 IEEE International Symposium on* (2010) pp. 1967 – 1970.

[7] S. H. Jo, T. Chang, I. Ebong, B. B. Bhadviya, P. Mazumder, and W. Lu, Nano Lett. **10**, 1297 (2010).

[8] Z. Q. Wang, H. Y. Xu, X. H. Li, H. Yu, Y. C. Liu, and X. J. Zhu, Adv. Funct. Mater. **22**, 2759 (2012).

[9] J. M. Cruz-Albrecht, T. Derosier, and N. Srinivasa, Nanotechnology **24**, 384011 (2013).

[10] A. D. Inglis, Y. Le Page, P. Strobel, and C. M. Hurd, J. Phys. C: Solid State Phys. **16**, 317 (1983).

[11] J. P. Strachan, J. J. Yang, R. Münstermann, A. Scholl, G. Medeiros-Ribeiro, D. R. Stewart, and R. S. Williams, Nanotechnology **20**, 485701 (2009).

[12] D.-H. Kwon, K. M. Kim, J. H. Jang, J. M. Jeon, M. H. Lee, G. H. Kim, X.-S. Li, G.-S. Park, B. Lee, S. Han, M. Kim, and C. S. Hwang, Nat. Nanotechnol. **5**, 148153 (2010).

[13] M. Marezio, D. B. McWhan, P. D. Dernier, and J. P. Remeika, J. Solid State Chem. **6**, 213 (1973).

[14] Y. Le Page and P. Strobel, J. Solid State Chem. **43**, 314 (1982).

[15] S.-G. Park, B. Magyari-Köpe, and Y. Nishi, IEEE Electr. Device L. **32**, 197 (2011).

[16] P. Deák, B. Aradi, and T. Frauenheim, Phys. Rev. B **83**, 155207 (2011).

[17] J. M. Knaup, J. Marx, and T. Frauenheim, Phys. Status Solidi RRL **8**, 549 (2014).

[18] J. Sanchez, F. Ducastelle, and D. Gratias, Physica A **128**, 334 (1984).

[19] D. Lerch, O. Wieckhorst, G. L. W. Hart, R. W. Forcade, and S. Müller, Model. Simul. Mater. Sc. **17**, 055003 (2009).

[20] G. Kresse and J. Furthmüller, Phys. Rev. B **54**, 11169 (1996).

[21] G. Kresse and J. Furthmüller, Comp. Mater. Sci. **6**, 15 (1996).

[22] P. E. Blöchl, Phys. Rev. B **50**, 17953 (1994).

[23] G. Kresse and D. Joubert, Phys. Rev. B **59**, 1758 (1999).

[24] J. P. Perdew, A. Ruzsinszky, G. I. Csonka, O. A. Vydrov, G. E. Scuseria, L. A. Constantin, X. Zhou, and K. Burke, Phys. Rev. Lett. **100**, 136406 (2008).

[25] The smallest possible symmetric cell was chosen for each configuration.

[26] S. Lany and A. Zunger, Phys. Rev. B **78**, 235104 (2008).

[27] S. Lany and A. Zunger, Phys. Rev. B **80**, 085202 (2009).

[28] S. Lany and A. Zunger, Phys. Rev. B **81**, 113201 (2010).

[29] J. Heyd, G. E. Scuseria, and M. Ernzerhof, J. Chem. Phys. **118**, 8207 (2003).

[30] J. Heyd, G. E. Scuseria, and M. Ernzerhof, J. Chem. Phys. **124**, 219906 (2006).

[31] S. Lany, private communication.

[32] H. J. Monkhorst and J. D. Pack, Phys. Rev. B **13**, 51885192 (1976).

[33] G. L. W. Hart, V. Blum, M. J. Walorski, and A. Zunger, Nat. Mater. **4**, 391 (2005).

[34] V. Blum, G. L. W. Hart, M. J. Walorski, and A. Zunger, Phys. Rev. B **72**, 165113 (2005).

[35] M. Stone, J. R. Stat. Soc. Ser. B **36**, 111 (1974).

[36] S. Harada, K. Tanaka, and H. Inui, J. Appl. Phys. **108**, 083703 (2010).

[37] J. Anderson and B. Hyde, J. Phys. Chem. Solids **28**, 1393 (1967).

[38] Assigning a formal oxidation state to these highly over-coordinated ions based on their neighbor count yields numbers that bear no connection to the electron population of the respective atoms. The empirical concept of 'oxidation state' fails in this context.

[39] L. Liborio, G. Mallia, and N. Harrison, Phys. Rev. B **79**, 245133 (2009).

[40] L. Liborio and N. Harrison, Phys. Rev. B **77**, 104104 (2008).

[41] A. C. M. Padilha, J. M. Osorio-Guillén, A. R. Rocha, and G. M. Dalpian, Phys. Rev. B **90**, 035213 (2014).

[42] J. M. Knaup, M. Wehlau, and T. Frauenheim, Phys. Rev. B **88**, 220101(R) (2013).

[43] K. Momma and F. Izumi, Journal of Applied Crystallography **44**, 1272 (2011).

[44] W. Humphrey, A. Dalke, and K. Schulten, J. Mol. Graphics **14**, 33 (1996).

[45] UNCLE is licensed by Materials Design. `info@materialsdesign.com`.